Respiratory Research

RESEARCH Open Access

YAP/TAZ-mediated nuclear membrane rupture in promoting senescence of skeletal muscle associated with COPD

Ge Gong[1,2], Shuping Shen[1], Shaoran Shen[1], Ran Wang[1], Tianping Zheng[1], Wei Xu[1*] and Jianqing Wu[1*]

Abstract

Patients with chronic obstructive pulmonary disease (COPD) often develop complications associated with sarcopenia; however, the underlying mechanisms remain unclear. Through a combination of in vitro and in vivo experiments, as well as bioinformatics analysis, our study identified YAP/TAZ as a key regulator of the aging phenotype in the skeletal muscle of COPD patients. In skeletal muscle affected by cigarette smoke-induced COPD, we observed significant reductions in YAP/TAZ levels, alongside markers indicative of skeletal muscle aging and dysfunction. Notably, overexpression of YAP/TAZ significantly improved these conditions. Our results suggest a novel mechanism whereby the maintenance of YAP/TAZ activity interacts with ACTR2 to preserve nuclear membrane integrity and reduce cytoplasmic dsDNA levels, thereby attenuating STING activation and cellular senescence. Additionally, we found that YAP is involved in the transcriptional regulation of the ACTR2 promoter region. Overall, preserving YAP/TAZ activity may help prevent skeletal muscle aging associated with COPD, representing a new strategy for intervening in COPD-related sarcopenia.

Clinical trial number

Not applicable.

Keywords COPD, Sarcopenia, YAP/TAZ, ACTR2, Nuclear membrane rupture, Senescence

Introduction

Chronic Obstructive Pulmonary Disease (COPD) is a complex clinical syndrome with systemic effects [1, 2]. Sarcopenia, an age-related progressive condition, is characterized by a decline in muscle mass, strength, or physiological function [3]. It is a significant comorbidity of COPD, with patients typically experiencing sarcopenia 15 to 20 years earlier than healthy individuals, at a prevalence rate of 15–40% [4]. Sarcopenia exacerbates lung function deterioration in COPD patients, leading to reduced quality of life, increased disability, and mortality [5, 6]. Despite its impact, the specific mechanisms underlying COPD-related sarcopenia remain unclear.

Studies have shown that in the pathogenesis of COPD, systemic inflammatory response, hypoxia, hypercapnia, oxidative and nitrosative stress, mitochondrial dysfunction, metabolic disorders, and epigenetic modifications are independent but interrelated mechanisms [7]. These factors collectively impact skeletal muscle homeostasis, resulting in a decline in muscle mass, strength, and function [8, 9]. Recent research indicates that COPD-related

*Correspondence:
Wei Xu
ann_hsu@njmu.edu.cn
Jianqing Wu
jwuny@njmu.edu.cn
[1]Key Laboratory of Geriatrics of Jiangsu Province, Department of Geriatrics, The First Affiliated Hospital with Nanjing Medical University, Nanjing, China
[2]Department of Geriatrics, Jinling Hospital, Affiliated Hospital of Medical School, Nanjing University, Nanjing, China

skeletal muscle alterations display an accelerated aging phenotype.

YAP and TAZ, two highly related transcriptional regulators (hereafter referred to as YAP/TAZ), serve as the nexus orchestrating the interplay between cellular mechanics, metabolism and developmental signaling cascades, allowing for cell and context-specific responses. The roles of YAP and TAZ in lung development may be associated with emphysema, and activating YAP/TAZ has been shown to mitigate the onset and advancement of emphysema in COPD [10].Skeletal muscle is a highly adaptable and regenerative tissue [11]. Recent evidence suggests that YAP/TAZ plays a crucial role in maintaining skeletal muscle function and homeostasis [12–14]. Studies on skeletal muscle aging have further demonstrated the involvement of YAP/TAZ in preserving muscle homeostasis [15] and potentially reversing the effects of muscle aging [16], yet the underlying molecular mechanisms are incompletely understood.

To propose new strategies for intervening in COPD-related sarcopenia, our research aims to clarify the significant role of YAP/TAZ in the accelerated aging process of COPD-related skeletal muscle, explore methods for regulating skeletal muscle aging, and identify potential therapeutic targets.

Materials and methods

Cigarette-smoke (CS) induced mouse model of COPD

C57BL/6 mice aged 6–8 weeks were procured from Beijing Vital River Laboratory Animal Technology Co., Ltd. and housed in a ventilated specific pathogen-free animal facility. All animal procedures were approved by the University Ethics Committee of Nanjing Medical University. Mice were kept on a 12-hour light/dark cycle with ad libitum access to food and water. The COPD mouse model was induced using the systemic animal smoke modeling system (CSM-AE, Tawang Technology, China) with Huangshan filter cigarettes from Anhui China Tobacco Industry Co., Ltd., which had a tar content of 10 mg and smoke carbon monoxide content of 11 mg. Real-time monitoring of total particulate matter (TPM) level and carbon monoxide (CO) concentration was conducted using an aerosol monitor (Casella, UK). The mice in the fumigation chamber were exposed to cigarette smoke with a TPM of 500 mg/m^3 and a CO level of approximately 288 ± 74 ppm, once a day for 2 h each time, 6 days a week for 24 consecutive weeks. Control mice were exposed to filtered air. Lung morphometric evaluation of lung sections were performed after 24 weeks of cigarette smoke exposure to confirm the successful establishment of the COPD model [17–19].

Grip force test

A handgrip dynamometer (KW-ZL, Nanjing, China) was used to assess the grip strength of the mice's forelimbs and hind limbs. Each mouse gripped a mesh rod connected to a force sensor with its limbs and was pulled back by its tail at a constant speed until the grip was released. The peak force (g) was automatically recorded by the sensor. Each mouse underwent three tests with a 2-minute rest interval between each test, and the average of the three measurements was taken as the grip strength [20]. This measurement was conducted weekly.

C2C12 cell culture and myotubes formation

C2C12 myoblasts derived from the China Infrastructure of Cell Line Resource were cultured in DMEM supplemented with 10% FBS. Upon reaching 80% confluence, the cells were induced to differentiate by incubation in DMEM with 2% horse serum for 4 days, with medium changes every other day. The fully differentiated myotubes were then utilized for subsequent experiments [17].

Cigarette smoke extract (CSE) Preparation

The smoke produced by 4–6 Huangshan cigarettes (Chinese tobacco from Anhui Industrial Co., Ltd., each containing 10 mg of caramel, 0.8 mg of nicotine, and 11 mg of carbon monoxide) was dissolved in DMEM medium. The pH was adjusted to approximately 7.4, and the solution was subsequently filtered using a 0.22 μm aseptic filter to create a reserve solution of CSE. The concentration of the original liquid CSE was calculated as follows: (nicotine 0.8 mg × number of cigarettes) / total volume. To account for the unmeasured loss during the ignition process and to standardize the concentration, the absorbance value at 320 nm was measured, targeting a value of 0.74 ± 0.05. The resulting diluted solution was regarded as the standardized CSE solution. For subsequent experiments, this solution was diluted as necessary, with the final CSE concentration determined using the formula: (CSE original liquid volume / total volume after dilution) × 100% [21, 22].

Overexpression of YAP and TAZ in C2C12 myotubes

Mouse overexpression vector negative control (OEcon) and YAP/TAZ-targeting overexpression vectors (OEYAP and OETAZ) were obtained from Weizhen Biotech (Shandong, China) and transfected into C2C12 myotubes using lipo3000 in vitro transfection reagent (ThermoFisher, Waltham, MA, USA). Transfection was carried out with 4 μg of plasmid following the manufacturer's protocol. The efficiency of transfection and protein expression were assessed after 48 h. Plasmids used in this study included YAP (pAV-CMV-P2A-GFP), TAZ (pAV-CMV-P2A-RFP) and ctrl (pAV-CMV-RFP).

Senescence-associated beta-galactosidase (SA-β-Gal) staining

Cell senescence was assessed using the SA-β-Gal staining kit. After stimulating C2C12 cells with 4% CSE for 96 h, the cells were washed three times with PBS and fixed for 15 min using 4% formaldehyde at room temperature. Following this, an additional wash with PBS was performed, and 1 ml of freshly prepared SA-β-Gal staining solution was applied. This solution consisted of solution A (10 μL), solution B (10 μL), staining solution C (930 μL), and X-Gal solution (50 μL), resulting in a final concentration of 1 mg/mL. The cells were then incubated overnight (16 h) in a CO_2-free incubator at 37 ℃ and observed under an ordinary optical microscope.

Adeno-associated virus serotype 9 (AAV9) production and intramuscular AAV injections

AAV9-YAP (NM_001171147.1), AAV9-TAZ (NM_001171147.1), and AAV9-con vectors harboring the CMV promoters were provided by Weizhen Biotechnology (Shandong, China), with AAV9 diluted to a concentration of 2×10^{13} viral genomes per milliliter in physiological saline. AAV9 was injected into the right quadriceps and gastrocnemius muscles. Prior to injection, the injection site was prepared by first removing hair with a hair clipper. Subsequently, the mouse quadriceps and gastrocnemius muscles were injected at 3 points using a micro-syringe, with 5 μl administered at each point. Finally, the area was disinfected with iodophor and allowed to dry.

Tissue collection and sample Preparation

Mouse lungs, quadriceps femoris, and gastrocnemius muscles were dissected and dried. For immunohistochemistry and immunofluorescence detection, the tissues were embedded in OCT reagent, stored in a -80 °C refrigerator, and sectioned at 10 μm thickness. Histological examination was then performed. Additionally, for immunoblotting analysis, tissue samples were snap frozen in liquid nitrogen immediately after collection.

Table 1 The source and Article number of the primary antibody

Name	Cat No	Source
YAP1	13582-1-AP	proteintech
TAZ	23306-1-AP	proteintech
cGAS	29958-1-AP	proteintech
STING	19851-1-AP	proteintech
ACTR2	10992-1-AP	proteintech
dsDNA	sc-58749	Santa Cruz
dystroglycan	11017-1-AP	proteintech
MYHC	A4963	Abclonal
P21	A22460	Abclonal

Histology analysis of the mouse lungs and skeletal muscles

Hematoxylin and eosin (H&E) staining was employed to assess the gross pathology of mouse lung and skeletal muscle, while MASSON staining was utilized to evaluate pulmonary fibrosis in mice. Emphysema was evaluated using the mean linear intercept (MLI) to measure cavity enlargement. Furthermore, the cross-sectional area (CSA) of muscle fibers was determined according to established protocols [23, 24].

Immunofluorescence (IF) staining

Mouse tissue sections were washed with ice-cold phosphate buffered saline (PBS), fixed with 4% paraformaldehyde, permeabilized with 0.1% Triton X-100 in PBS, and blocked with 5% bovine serum albumin. Following these steps, the sections were incubated with primary and secondary antibodies, and nuclei were stained with DAPI, which were then visualized using a digital pathology slide scanner (Panoramic 250 MIDI, 3DHISTECH, Hungary). To minimize potential bias in the experimental results, individuals conducting the immunofluorescence experiments were blinded.

Western blot analysis

After lysing the mouse tissue and cell samples in RIPA buffer, the protein concentration in the supernatant was determined using the BCA method. Subsequently, equal amounts of protein were loaded onto SDS-PAGE gels for electrophoresis. The separated proteins were then transferred to a polyvinylidene fluoride (PVDF) membrane using the electroblotting technique. Following this, the membrane was blocked with QuickBlock™ Western (Beyotime, p0252), and both primary and secondary antibodies were incubated. The immunoblot was visualized using an ultrasensitive ECL detection reagent (Vazyme Biotech, Nanjing, China) and subsequently analyzed with ImageJ software. Specific details regarding the primary antibodies are provided in Table 1.

Statistical analysis

All data were statistically analyzed using SPSS 22.0 software. Normally distributed data were presented as mean ± standard deviation ($\bar{x} \pm s$), and a t-test was employed to compare the two groups. Differences among the four groups were evaluated using one-way analysis of variance (ANOVA), with pairwise comparisons conducted using Tukey's post hoc test. A significance level of $P < 0.05$ was considered statistically significant, where $^{*}P < 0.05$, $^{**}P < 0.01$, $^{***}P < 0.001$, $^{****}P < 0.0001$. Graphs were created using GraphPad Prism 10 software (GraphPad Software, La Jolla, CA, USA).

Results

COPD mouse model induced by CS exposure exhibiting skeletal muscle dysfunction

To investigate COPD-related sarcopenia, a smoke-exposed mouse model of COPD was developed and validated after 24 weeks of exposure. Mice in the smoke exposure group exhibited alveolar fusion expansion, increased MLI, inflammatory cell infiltration, airway fibrosis, and remodeling compared to the control group (Fig. 1A, B, C).

Weekly assessments were conducted on body weight, forelimb grasping strength, and limb grasping strength in the mice. Body weight reduction in the smoke-exposed group was evident from the fourth week post-exposure, with forelimb grip strength declining from the first week, and limb grip strength decreasing from the third week. Subsequent dissection of quadriceps and gastrocnemius muscles revealed significantly lower muscle weights in the smoke-exposed group compared to controls (Fig. 1D, E, F, G). H&E staining of muscles indicated altered muscle morphology, with reduced skeletal muscle and muscle fiber CSA in CS-exposed mice, along with the appearance of cavities in muscle fibers (Fig. 1H, I). In conclusion, the COPD model induced by CS exposure displays characteristics of skeletal muscle dysfunction.

Decreased YAP/TAZ expression and increased Senescence-Related protein expression in vitro and in vivo

Following the successful establishment of a COPD mouse model through smoke exposure, we observed a notable decrease in the expression of YAP/TAZ in the quadriceps and gastrocnemius muscles of the model mice (Fig. 2A). Western blot analysis revealed a significant increase in P21 levels and a decrease in MYHC levels (Fig. 2B). Additionally, SA-β-Gal staining indicated that the skeletal muscle of the CS group exhibited signs of senescence (Fig. 2C), and IF staining demonstrated reduced

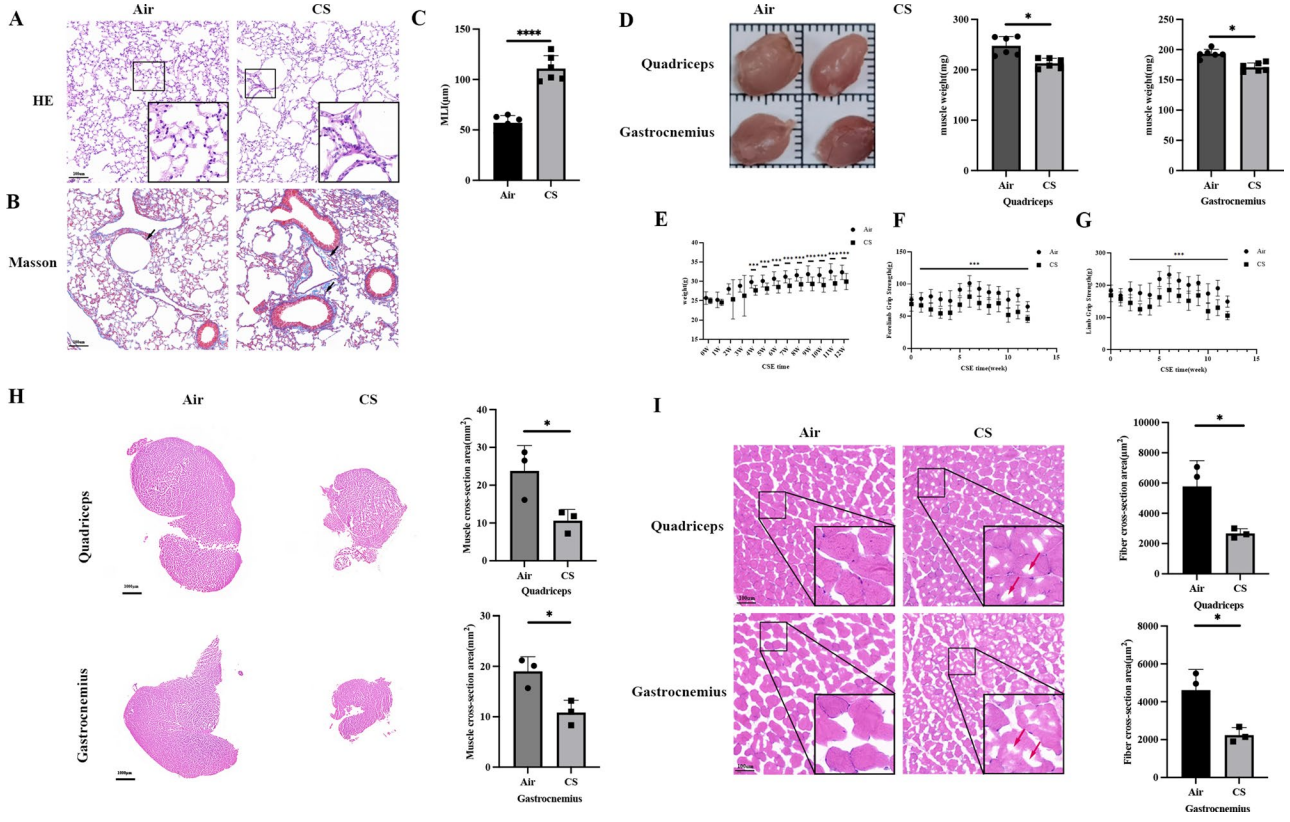

Fig. 1 The mouse model of *COPD* with skeletal muscle dysfunction was developed. Following 24 weeks of CS exposure, **A**. H&E staining revealed that the lung tissue structure in the CS group exhibited disorganization, thickening of alveolar walls, destruction of some alveoli, and infiltration of inflammatory cells in bronchial walls, alveoli, and interstitial cavities, whereas the lung tissue morphology in the control group appeared normal with clearly visible alveoli and absence of inflammatory cell infiltration. **B**. Masson staining showed significant collagen deposition and severe fibrosis in the lung tissue of the model group (black arrows); in contrast, the lung tissue structure of the control group appeared normal without typical fibrosis. **C**. The mean linear intercept (MLI) was notably higher in the model group compared to the control group. **D**. The quadriceps and gastrocnemius muscles of mice exhibited significant reduction in weight and size after 24 weeks of CS induction. **E**, **F**, **G**. Changes in mice body weight (**E**), forelimb *grip* strength (**F**), and limb *grip* strength (**G**) were observed after 12 weeks of modeling. **H**, **I**. H&E staining of skeletal muscle revealed a marked reduction in cross-sectional area of skeletal muscles and muscle fibers in the CS group, with disorganized arrangement, irregular shape, and some fibers showing cavity atrophy (red arrows); in contrast, the control group exhibited neatly arranged muscle fibers. ($^{*}P<0.05$, $^{**}P<0.01$, $^{***}P<0.001$, $^{****}P<0.0001$)

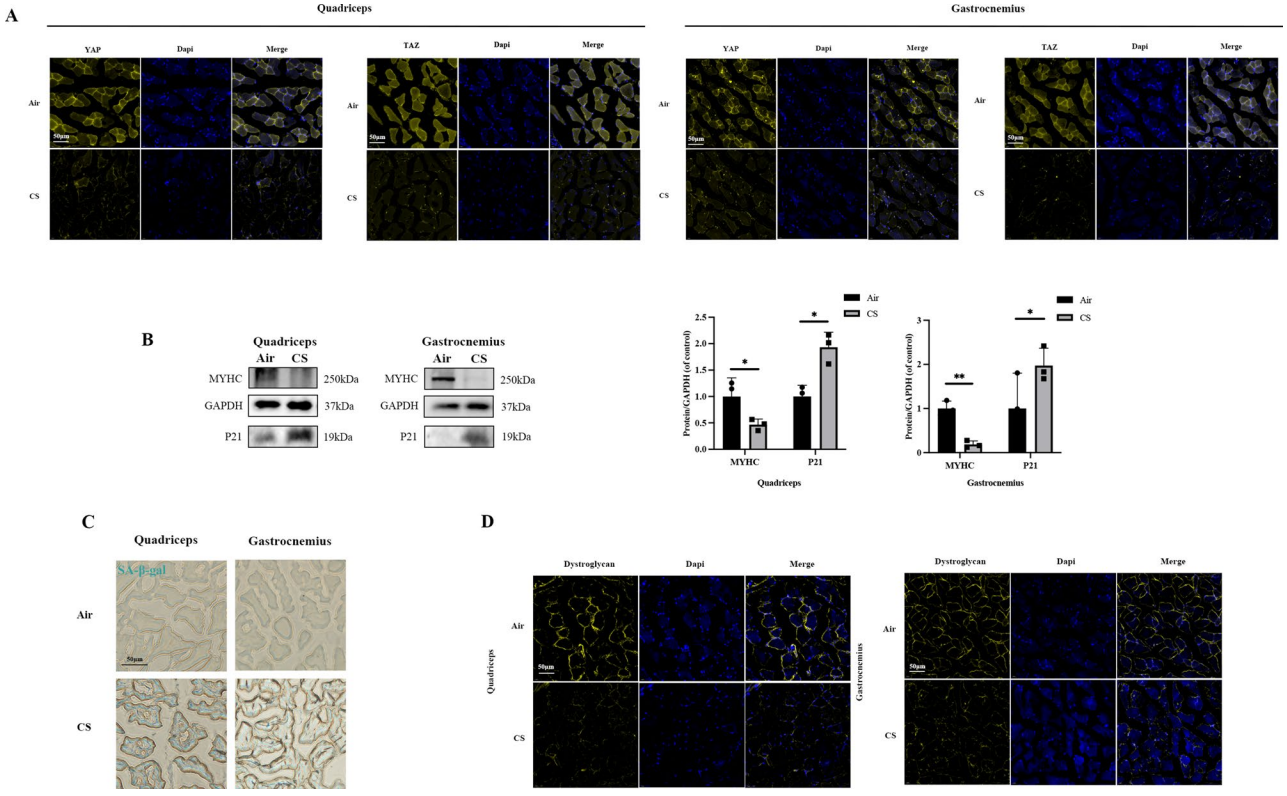

Fig. 2 Decreased YAP/TAZ expression and increased senescence-related protein expression in the skeletal muscles of the *mouse* model. **A**. Immunofluorescence analysis revealed a significant decrease in the expression of YAP/TAZ in the quadriceps and gastrocnemius muscles of mice in the cigarette smoke (CS) group. **B**. Western blot analysis indicated a significant decrease in MYHC expression and *an* increase in P21 expression in the CS group compared to the control group. **C**. SA-β-Gal staining indicated an increase in skeletal aging in mice exposed to CS, as evidenced by the blue staining. **D**. Immunofluorescence results demonstrated a significant decrease in dystroglycan expression in the CS group compared to the control group. ($^{*}P < 0.05$, $^{**}P < 0.01$, $^{***}P < 0.001$, $^{****}P < 0.0001$)

dystroglycan expression in the skeletal muscle of the CS group (Fig. 2D).

To investigate the impact of cigarette smoke exposure on myotube cells, C2C12 myotubes were subjected to CSE. The results showed that after 24 h of CSE exposure, there was a gradual decrease in the expression of YAP and TAZ along with the increasing concentration, while γ.H2AX expression increased (Fig. 3B). Notably, concentrations of 6% CSE and above led to significant cell death when observed under a microscope (Fig. 3A). In cases where cell death did not occur, exposure to 4% CSE for 48 h resulted in a significant alteration in YAP/TAZ expression, accompanied by a decrease in MYHC and an increase in γ.H2AX compared to the control group (Fig. 3C).

AAV9-Mediated YAP/TAZ overexpression preventing senescence of skeletal muscles in mice exposed to CS

To investigate the specific role of YAP/TAZ in skeletal muscle, we developed a recombinant overexpression plasmid containing mouse YAP/TAZ, which was then packaged with AAV9 and injected into the skeletal muscles (quadriceps and gastrocnemius) for evaluation after 12 weeks. Immunofluorescence analyses revealed higher YAP/TAZ immunofluorescence intensity by AAV9-YAP/TAZ administration compared to the contralateral limb injected with AAV9-con (Fig. 4A, B).

An interesting phenomenon was uncovered during our investigation. Immunofluorescence analysis revealed a significant decrease in the expression of YAP/TAZ in both the cytoplasm and nucleus of the CS group and CS + AAV9-con group compared to the normal control group. However, this phenomenon was reversed upon the overexpression of YAP/TAZ (Fig. 4C, D).

Limb grip strength was assessed twelve weeks after the injection of AAV9-overexpressing YAP/TAZ into the quadriceps and gastrocnemius muscles of COPD mouse model. In the CS + AAV9-con group, the limb grip strength of COPD mice decreased significantly. Compared to the control group, limb grip strength in the CS + AAV9-YAP and CS + AAV9-TAZ groups showed a significant increase (Fig. 5B), whereas no significant change was observed in forelimb grip strength (Fig. 5C).

Additionally, the weight of the quadriceps and gastrocnemius muscles showed significant increases in the CS + AAV9-YAP and CS + AAV9-TAZ groups,

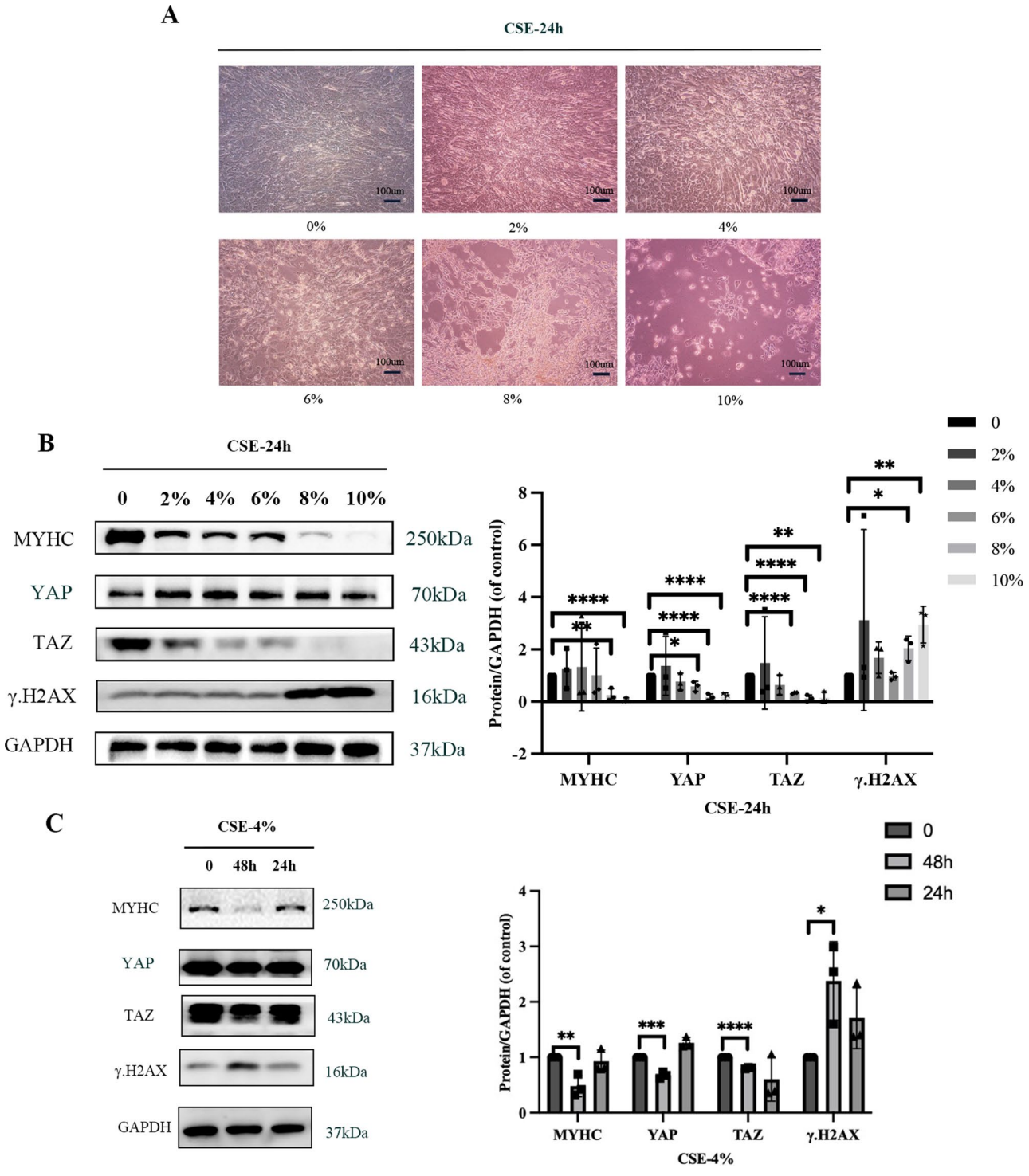

Fig. 3 Decreased YAP/TAZ expression and increased senescence-related protein expression in cigarette smoke extract (CSE) exposed C2C12 myotube cells. **A**. Microscopic observation of C2C12 myotubes after 24 h of exposure to CSE *revealed* that increased CSE concentration *correlated* with increased cell death. **B**. With rising CSE concentration, the expression of YAP/TAZ gradually *decreased*, while the expression of the nuclear DNA damage marker γ.H2AX gradually *increased*, and the expression of MYHC gradually *declined*. Notably, after 24 h of exposure to high-concentration CSE, significant changes in related protein expressions *were* observed. **C**. Following 48 h of stimulation with 4% CSE, the expression changes of YAP/TAZ, γ.H2AX, and MYHC *became* more pronounced compared to the 24-hour mark. ($^{*}P < 0.05$, $^{**}P < 0.01$, $^{***}P < 0.001$, $^{****}P < 0.0001$)

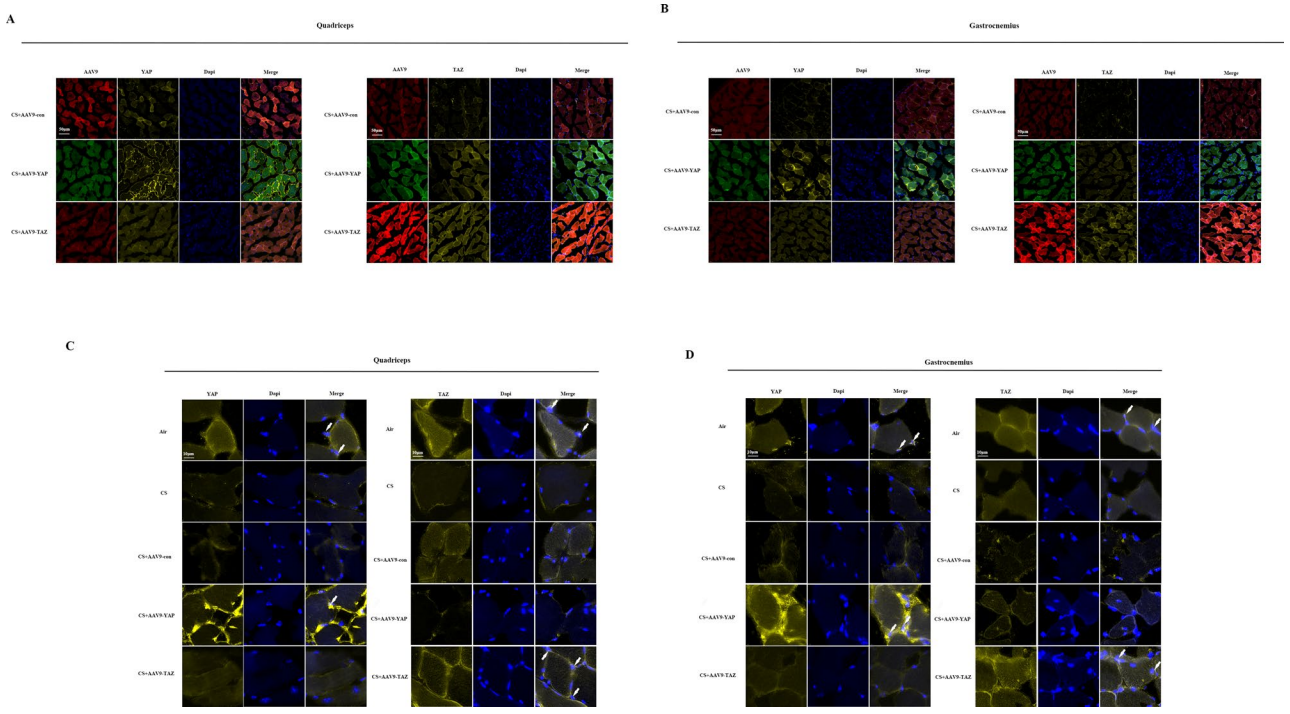

Fig. 4 YAP/TAZ expression after AAV9-YAP/TAZ injection into skeletal *muscles*. **A**.**B**. Immunofluorescence analysis revealed an increase in YAP/TAZ expression following the injection of AAV9-YAP and AAV9-TAZ into the quadriceps and gastrocnemius muscles, as compared to the control group. **C**.**D**. A reduction in YAP/TAZ expression in the nucleus of the CS group was observed when compared to the normal control group. However, *following* injection of AAV9-YAP and AAV9-TAZ, a significant increase in YAP/TAZ expression *was noted* in the nucleus (white arrows)

respectively (Fig. 5A). Investigation of muscle histology is a routine approach to study muscle function. H&E staining of skeletal muscle revealed a notable increase in the CSA of both skeletal muscle (Fig. 5D) and muscle fibers (Fig. 5E) in the YAP/TAZ overexpression group. Conversely, the control group exhibited disorganized skeletal muscle fibers with irregular shapes, along with some fibers showing cavities and signs of atrophy. Notably, the YAP/TAZ overexpression group demonstrated a significant reduction in myofiber cavities, with cell nuclei shifting inward (Fig. 5E). SA-β-Gal staining revealed that YAP/TAZ overexpression rescued the skeletal muscle senescence (Fig. 5G). Moreover, compared to the control group, the expression of P21 decreased significantly in the CS + AAV9-YAP and CS + AAV9-TAZ groups, while the expression of MYHC and dystroglycan increased significantly (Fig. 5F, H).

YAP/TAZ overexpression rescuing senescence of skeletal muscle exposed to CSE, with the mechanism being probably related to STING pathway

To investigate the specific role of YAP/TAZ in COPD-related skeletal muscle aging, we utilized immunofluorescence to examine proteins associated with the cGAS-STING pathway. Cytosolic DNA derived from host genome (dsDNA, including leaked/ damaged nuclear DNA from chromosome instability), are powerful activators for the STING cascade. Our results showed there was a significant increase in dsDNA expression within the cytoplasm of skeletal muscle in the COPD mouse model. Conversely, the overexpression of YAP/TAZ led to a notable reduction in cytoplasmic dsDNA expression (Fig. 6A, B). Additionally, we observed a correlation between the expression of dsDNA in the cytoplasm and YAP/TAZ levels. Interestingly, the expression of dsDNA was found to be inversely related to the levels of YAP/TAZ. Moreover, STING expression was notably increased in the quadriceps and gastrocnemius muscles of COPD mice compared to the control group. Following the overexpression of YAP/TAZ in COPD model mice, STING expression in skeletal muscle decreased significantly (Fig. 6C, D). However, there was no significant difference in cGAS expression between the groups (Fig. 6E, F).

In myotube cells exposed to CSE, there was a significant decrease in YAP/TAZ levels. Subsequently, C2C12 myotube cells after 4% CSE exposure for 48 h were chosen as the modeling condition for further experiments in vitro. Following YAP/TAZ effective overexpression by plasmid vectors (OE-YAP and OE-TAZ) in CSE-exposed myotube cells, SA-β-Gal staining revealed that YAP/TAZ overexpression rescued cell senescence (Fig. 7B). After manipulation of YAP/TAZ overexpression, MYHC and

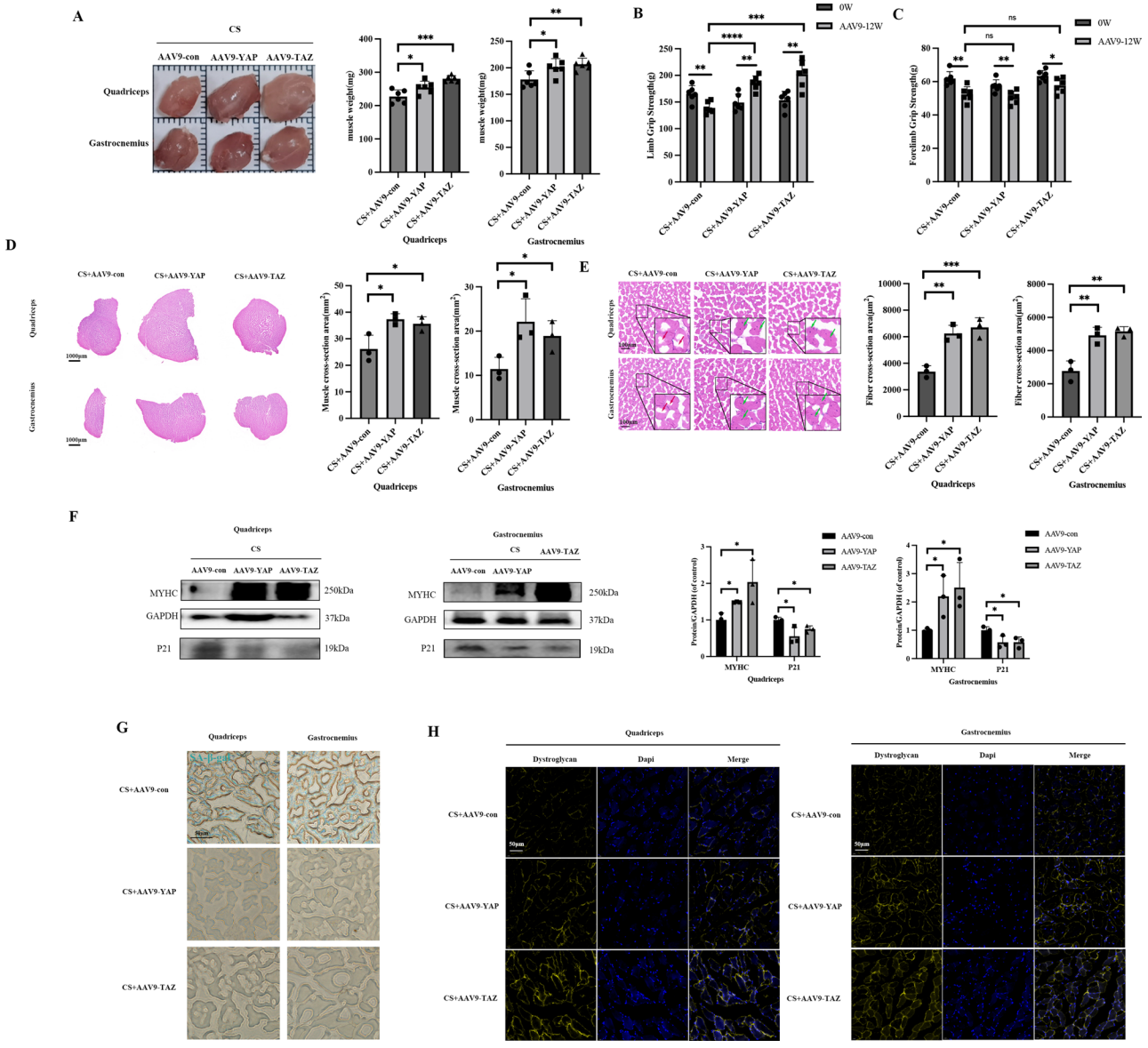

Fig. 5 AAV9-mediated YAP/TAZ overexpression prevented dysfunctional skeletal muscles in mice exposed to cigarette smoke (CS). **A.B.C**. Mice overexpressing YAP/TAZ showed noticeable increases in the weight and size of skeletal muscles (**A**), as well as improvements in forelimb gripping force (**B**) and limb gripping force (**C**). **D**.**E**. H&E staining of skeletal muscle revealed a notable increase in the cross-sectional area of both skeletal *muscles* and muscle fibers in the YAP/TAZ overexpression group. Conversely, the control group exhibited disorganized skeletal muscle fibers with irregular shapes, along with some fibers showing cavities and signs of atrophy (red arrows). Notably, the YAP/TAZ overexpression group demonstrated a significant reduction in myofiber cavities, with three or more nuclei observed within the fibers (green arrows) (**E**). **F**. Western Blot analysis showed a significant increase in MYHC expression and a decrease in P21 expression in the CS + AAV9-YAP/TAZ group compared to the control group. **G**. SA-β-gal staining revealed that YAP/TAZ overexpression led to a substantial reduction in senescent skeletal muscles relative to the control group (blue). **H**. Immunofluorescence results further demonstrated a significant increase in dystroglycan expression in the CS + AAV9-YAP/TAZ group compared to the control group. ($^{*}P < 0.05$, $^{**}P < 0.01$, $^{***}P < 0.001$, $^{****}P < 0.0001$)

ACTR2 expression increased, while the expression of P21 and STING decreased (Fig. 7A).

To investigate whether dsDNA was derived from the nucleus due to the breakdown of the nuclear membrane, we examined the morphology of the nuclear membrane using transmission electron microscopy. Our observations revealed that exposure to CSE resulted in an irregularly shaped nuclear membrane in myotube cells, with indentations and a disrupted nuclear lamina. Interestingly, overexpression of YAP/TAZ was able to ameliorate these effects, improving the indentations in the nuclear membrane and preventing the breakage of the nuclear lamina (Fig. 7C).

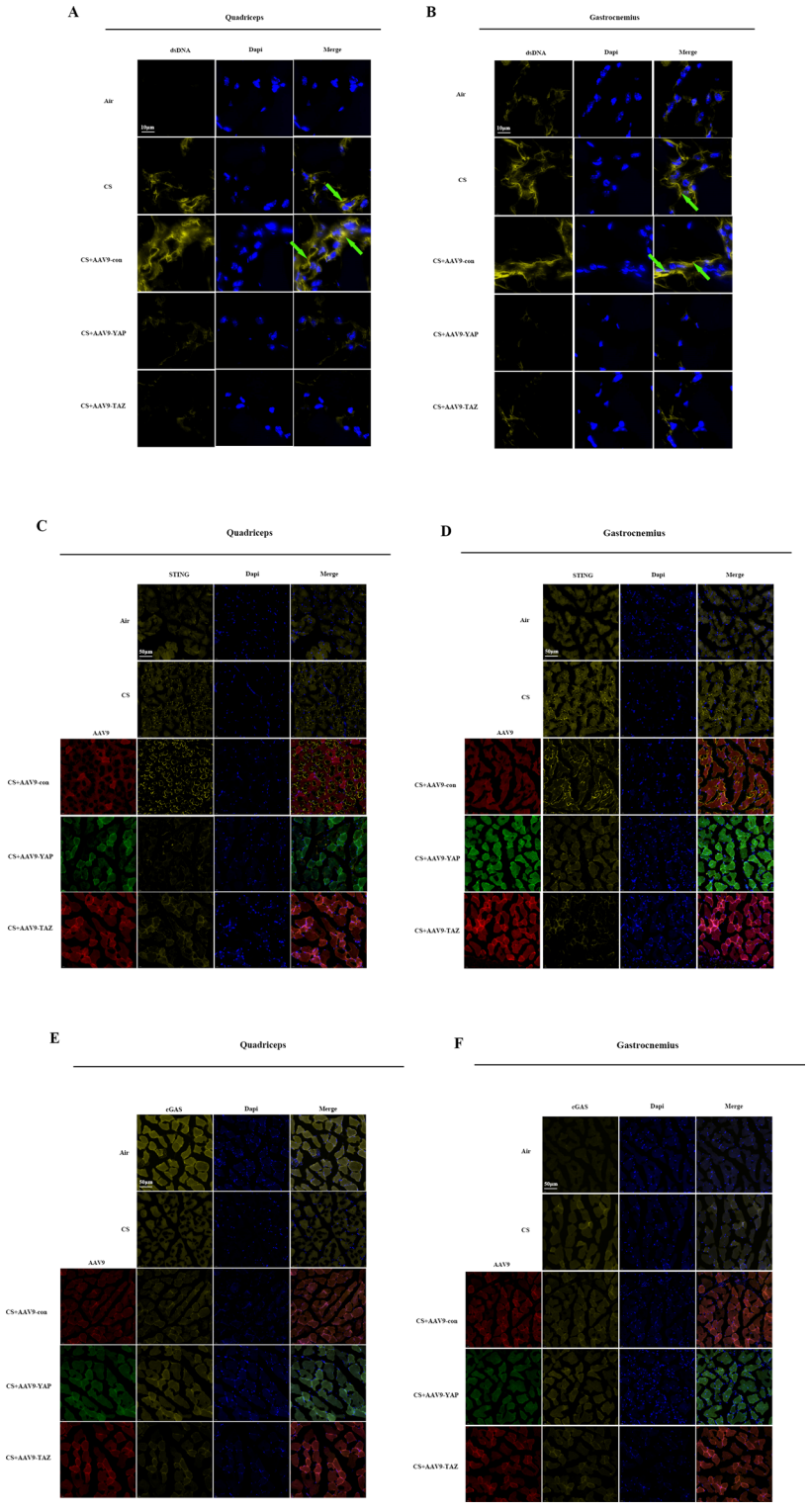

Fig. 6 Expression of dsDNA, cGAS and STING in skeletal muscles of each group. **A**.**B**. There was a significant increase in dsDNA expression (green arrows) in the cytoplasm of quadriceps and gastrocnemius muscles of mice in the CS group compared to the normal control group. However, this expression was significantly reduced in the CS + AAV9-YAP and CS + AAV9-TAZ groups compared to the CS + AAV9-con group. **C**.**D**. Immunofluorescence analysis revealed no significant differences in cGAS expression among the groups. **E**.**F**. In comparison to the control group, STING expression was notably elevated in the quadriceps and gastrocnemius muscles of mice in the CS group. This expression was significantly reduced in the CS + AAV9-YAP and CS + AAV9-TAZ groups compared to the CS + AAV9-con group

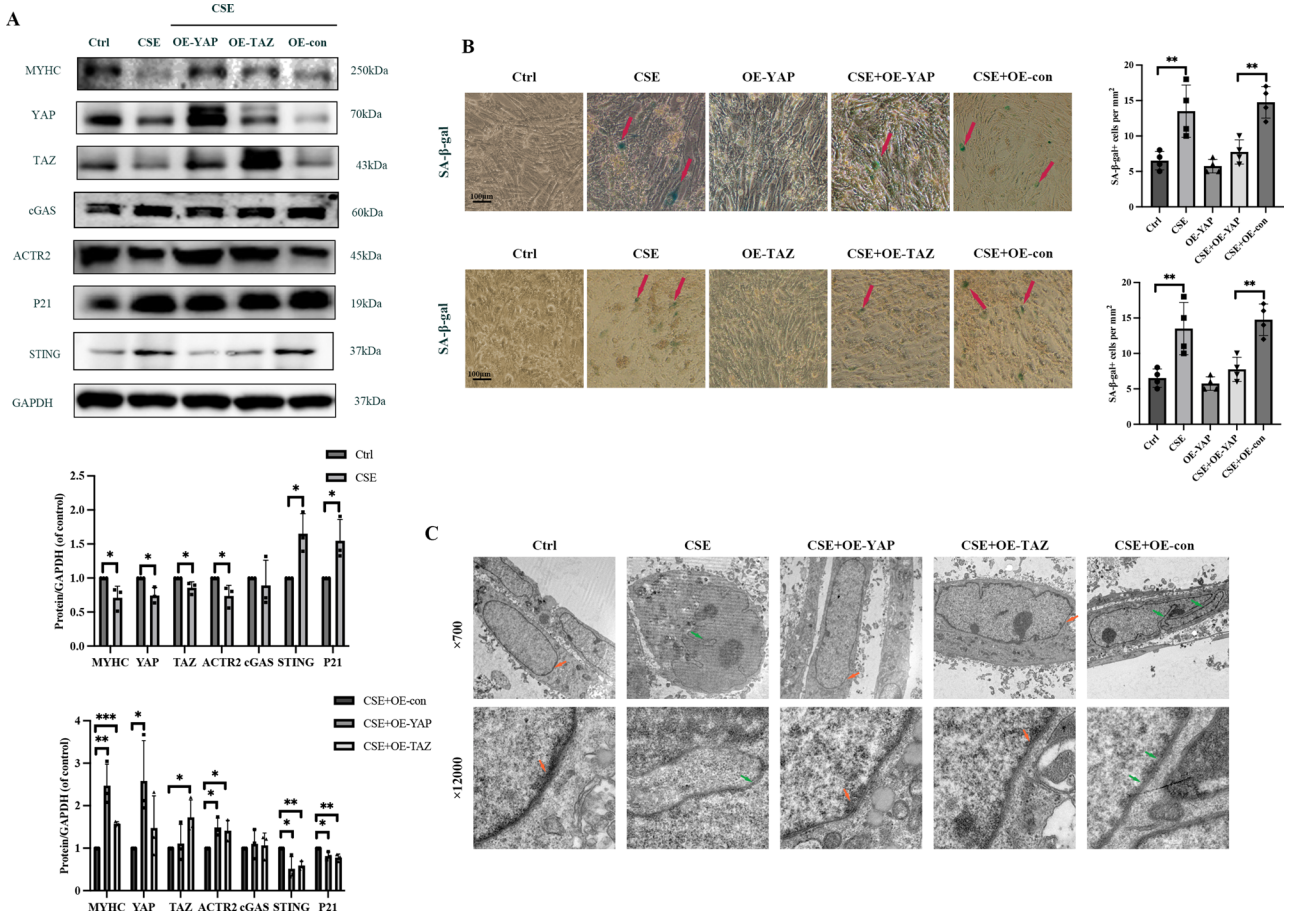

Fig. 7 The rescue of skeletal muscle aging following the overexpression of YAP/TAZ through STING pathway. (**A**) Western blot analysis revealed that 48 h post-transfection of the YAP/TAZ plasmid into C2C12 myotubes, the expression levels of YAP/TAZ were significantly elevated compared to the control group. Following CSE exposure, the expressions of YAP/TAZ, MYHC, and ACTR2 were notably decreased in comparison to the control group, while the expressions of STING and P21 were significantly increased. After the overexpression of YAP/TAZ, there was a marked increase in the expression of MYHC and ACTR2 in C2C12 myotube cells exposed to CSE, alongside a significant decrease in the expression of P21 and STING; however, cGAS exhibited no significant changes. (**B**) SA-β-gal staining indicated a significant increase in senescent cells within C2C12 myotubes *exposed to* CSE, whereas overexpression of YAP/TAZ led to a significant reduction in senescent cells compared to the control group (red arrow). (**C**) Examination of C2C12 myotube cells via transmission electron microscopy revealed that the irregularly shaped nuclei of myotube cells exposed to CSE exhibited inward depression, as well as thinning and fracturing of the nuclear fiber membrane (green arrow). Overexpression of YAP/TAZ ameliorated these alterations, resulting in reduced nuclear membrane depression and thickening of the nuclear lamina (orange arrow). ($^{*}P < 0.05$, $^{**}P < 0.01$, $^{***}P < 0.001$, $^{****}P < 0.0001$)

YAP-Mediated transcriptional regulation of ACTR2

Based on data sets GSE100281 and GSE27536, KEGG enrichment analyses revealed that the expression pattern of YAP/TAZ was significantly associated with multiple gene modules of actin cytoskeleton regulation Fig. 8A). Meanwhile, the expression level of ACTR2 was found to be consistent with YAP in CSE-exposed C2C12 myotubes Fig. 7A) and COPD model mice Fig. 8C, D). Examination of CHIP-seq data from GSM1542533 and GSM1515738 datasets indicated a link between YAP and ACTR2 Fig. 8B). This relationship was further validated through a dual-luciferase assay, revealing YAP's involvement in the transcriptional regulation of the ACTR2 promoter region. Subsequent segmentation of the ACTR2 promoter region into four fragments exposed multiple binding sites for both YAP and the ACTR2 promoter (Fig. 8E, F).

Discussion

Compared to healthy individuals of the same age, patients with COPD often experience sarcopenia at a younger age, which is associated with a worse prognosis [25]. Various factors contribute to skeletal muscle dysfunction in COPD patients, including systemic inflammatory response, hypoxia, hypercapnia, oxidative and nitrosative stress, mitochondrial dysfunction, metabolic disorders, and epigenetic modifications [7, 26].

Our study identified age-associated changes in the skeletal muscle of COPD mouse model and CSE-exposed myotube cells. Importantly, the overexpression of YAP/TAZ effectively alleviated muscle atrophy and

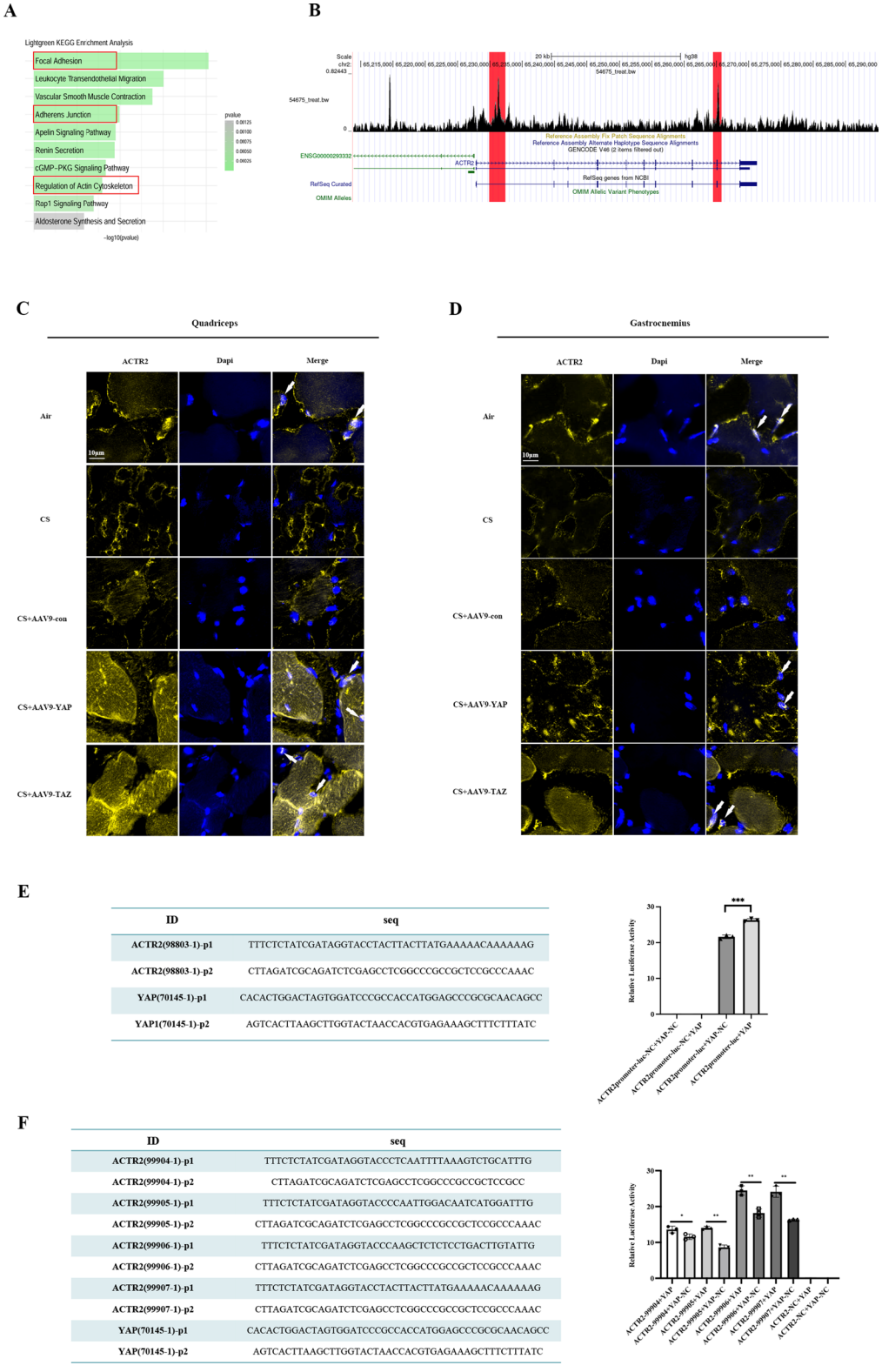

Fig. 8 (See legend on next page.)

(See figure on previous page.)

Fig. 8 YAP-mediated transcriptional regulation of ACTR2. **A**. Analysis of the GSE100281 and GSE27536 datasets through KEGG enrichment *revealed* a significant association between the actin cytoskeleton regulation-related gene module (red box) and the expression pattern of YAP/TAZ. **B**. Analysis of CHIP-seq data from the GSM1542533 and GSM1515738 datasets *suggested* a relevant relationship between YAP and ACTR2. **C**.**D**. Immunofluorescence analysis revealed a significant decrease in ACTR2 expression (white arrows) in the cell nuclei of quadriceps and gastrocnemius muscles of mice in the CS group compared to the normal control group. Conversely, ACTR2 expression was notably increased in the nuclei of quadriceps and gastrocnemius muscles in the CS + AAV9-YAP and CS + AAV9-TAZ groups compared to the CS + AAV9-con group. **E**. The dual-luciferase reporter gene experiment indicated that YAP *was* involved in the transcriptional regulation of the ACTR2 promoter region. **F**. Further predictions based on truncated sequence analysis of the YAP binding to the ACTR2 promoter suggested that YAP *interacted* with multiple regulatory binding sites for ACTR2 transcription. ($^{*}P < 0.05$, $^{**}P < 0.01$, $^{***}P < 0.001$, $^{****}P < 0.0001$)

senescence, as evidenced by the aging markers P21 and γ.H2AX [27, 28], both in vivo and in vitro, emphasizing the role of YAP/TAZ, key downstream effectors of the Hippo pathway, in modulating the aging phenotype of skeletal muscle affected by COPD. Previous studies have demonstrated that YAP/TAZ activity declines during the physiological aging of skin fibroblasts and vascular smooth muscle cells. This decline can be mimicked through the genetic inactivation of YAP/TAZ, resulting in accelerated aging. Conversely, maintaining YAP function can rejuvenate senescent cells and prevent characteristics associated with physiological aging and accelerated aging-related characteristics by Hippo-independent mechanisms [9, 29, 30]. Additionally, a proteomic study on single muscle fibers revealed that YAP protein expression in slow muscle fibers was twice as high in young subjects compared to fast muscle fibers, while YAP expression levels in elderly subjects were significantly reduced in both muscle fiber types [31]. These findings suggest that muscle fiber type-dependent variations in YAP/TAZ regulation may play a critical role in the senescence phenotype of skeletal muscle.

Studies have demonstrated that the loss of YAP and TAZ leads to an increased pro-inflammatory state through cGAS-STING signaling [32]. The cGAS-STING pathway is an emerging innate immune signaling pathway that not only links cellular damage to inflammatory responses but also drives chronic inflammation and functional decline associated with aging [33]. While STING is present in various muscle tissues, its relationship with skeletal muscle has not been extensively studied. Mechanistically, in aging muscle cells, endogenous cytoplasmic dsDNA fragments serve as potent pro-inflammatory stimuli and ligands for cGAS. Upon binding to dsDNA, cGAS synthesizes cGAMP using ATP and GTP, which subsequently activates STING. Activated STING recruits the kinase TBK1, phosphorylates downstream IRF3 and NF-κB, induces type I interferon, and ultimately regulates the production of the senescence-associated secretory phenotype, thereby controlling cellular aging [27; 28]. In this study, we observed a significant increase in dsDNA and STING expression within the cytoplasm of skeletal muscle both in vivo and in vitro. Following the overexpression of YAP/TAZ, levels of dsDNA and STING significantly decreased, while cGAS levels did not exhibit any significant change. This observation may be attributed to the activation of STING by cGAS through the formation of cGAMP upon binding to dsDNA in the cytoplasm. Furthermore, evidence suggests that STING activation can occur independently of cGAS under specific conditions, supported by the direct binding of STING to exogenous ligands, indicating that cGAS is not the sole upstream regulator of STING [34].More convincing evidence is needed to establish this signaling axis.

In the current study, we observed irregular nuclear shapes, inward appearances of the nuclear membrane, and the fragmentation and disappearance of the nuclear lamina in myotube cells exposed to CSE as analyzed by transmission electron microscopy. Overexpression of YAP/TAZ mitigated these effects. We speculate that dsDNA was released from the nucleus due to the breakdown of the nuclear membrane. Recent studies have demonstrated that YAP/TAZ plays a critical role in maintaining the integrity of the nuclear membrane during the natural aging process of fibroblasts and vascular smooth muscle cells. This function of YAP/TAZ is essential for supporting the nuclear lamina, as evidenced by the expression of Lamin B1 and the formation of perinuclear actin caps regulated by ACTR2 [29, 35, 36]. Our research revealed a significant decrease in the expression of YAP/TAZ in the cytoplasm and nucleus of COPD-related skeletal muscles and myotubes, along with a reduction in ACTR2 levels within the nucleus. These findings confirm the diminished nuclear membrane invagination and fragmentation of the nuclear lamina in COPD-related skeletal muscle and myotube cells. YAP/TAZ exerts its protective role on the nuclear membrane through ACTR2. Furthermore, our study validated the regulatory relationship between YAP and ACTR2 through bioinformatics analysis and dual-luciferase assays. As summarized in our proposed model (Fig. 9), the current study supports the possible mechanism by which maintenance of YAP/TAZ activity interacts with ACTR2, preserves nuclear membrane integrity, and reduces cytoplasmic dsDNA, thereby mitigating STING activation and alleviating cellular aging.

Previous studies have demonstrated that exercise training and nutritional interventions can improve skeletal muscle function, delay the onset of sarcopenia, and significantly enhance lung function in patients with COPD

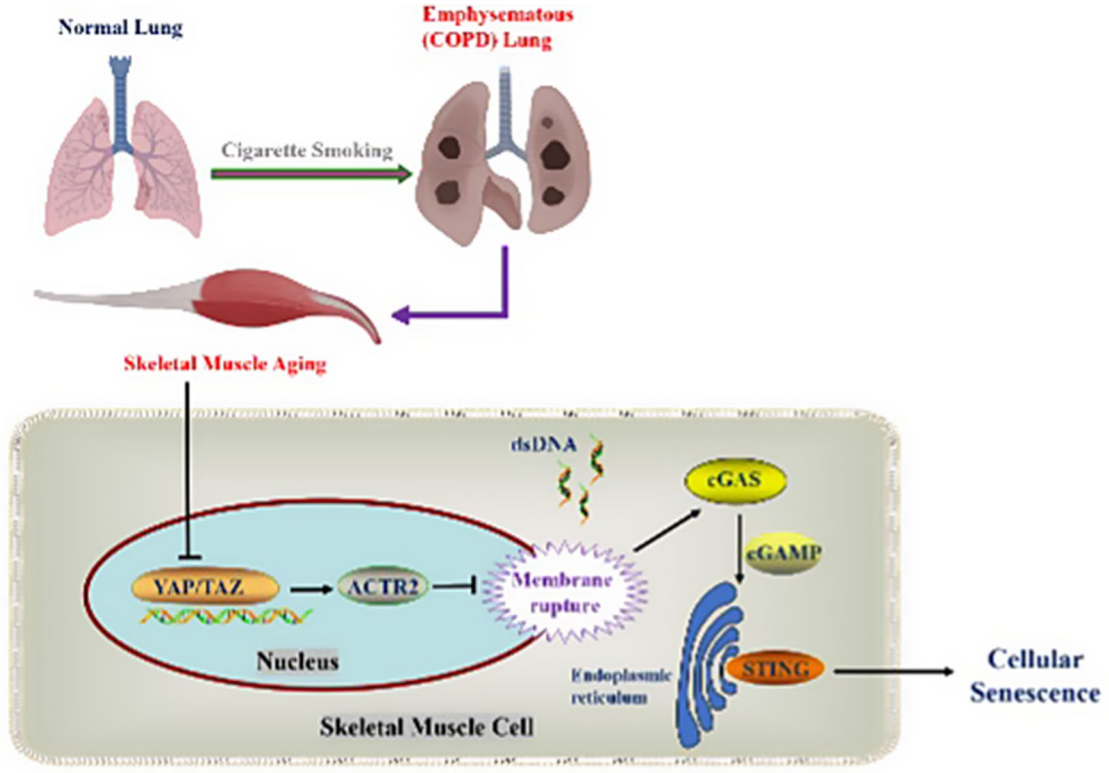

Fig. 9 Schematic diagram of the mechanism by which YAP/TAZ protects against skeletal muscle aging related to COPD. In the COPD model exposed to CS, the expression of YAP/TAZ decreased, which correspondingly resulted in a reduction of ACTR2 expression in the nucleus. Following the rupture of the nuclear membrane, there was an increase in dsDNA in the cytoplasm, which subsequently led to an upregulation of STING expression, ultimately promoting skeletal muscle senescence

[37, 38]. Our research focuses exclusively on the aging of skeletal muscle related to COPD; however, addressing the overall improvement of COPD is essential for enhancing patient outcomes. At that time, we did not investigate the tools for assessing changes in mouse lung function, and it is necessary to enhance overall muscle function in mice to improve COPD prognosis. We acknowledge this limitation. In future work, we will design YAP/TAZ activators specifically targeting skeletal muscles to enhance the function of the entire skeletal muscle system and improve the prognosis of COPD.

Conclusions

In our current investigation, we demonstrate that YAP/TAZ is a crucial regulator of the senescence phenotype in the skeletal muscle of a COPD mouse model. Our study also suggests a novel mechanism by which the maintenance of YAP/TAZ activity interacts with ACTR2, preserves nuclear membrane integrity, and reduces cytoplasmic dsDNA, thereby mitigating STING activation and alleviating cellular aging. Future researchfocusing on YAP/TAZ activity in COPD-related skeletal muscle disorders is warranted to validate our findings and to further explore the therapeutic potential for manipulating YAP/TAZ in this context.

Supplementary Information

The online version contains supplementary material available at https://doi.org/10.1186/s12931-025-03170-4.

Supplementary Material 1

Acknowledgements

Not applicable.

Author contributions

GG: Writing, Validation, Analysis, Drawing. ShuS: Visualization, Validation. ShaoS: Methodology, Software. RW: Visualization, Validation. TZ: Investigation. WX: Validation, Methodology, Investigation, Funding acquisition. JW: Supervision, Funding acquisition, Formal analysis. All authors reviewed the manuscript.

Funding

This study was supported by research grants from the National Natural Science Foundation of China (82471605, 82171576), Jiangsu Province Capability Improvement Project through Science, Technology and Education (No. CXZX202228 to Jianqing Wu), Major Natural Science Research Projects in Colleges and Universities of Jiangsu Province (No. 22KJA320003 to Wei Xu), Applied research project unit of geriatric medicine clinical technology in Jiangsu Province (LD2022001), Jiangsu Province Elderly Health Scientific Research Project (LKM2024021).

Data availability
The datasets used or analyzed during the current study are available from the corresponding author on reasonable request.

Declarations

Ethics approval and consent to participate
This study was approved by the Ethics Committee of the First Affiliated Hospital of Nanjing Medical University (approved protocol number: 2023-SR-530). The manuscript does not contain human subjects.

Consent for publication
Not applicable.

Competing interests
The authors declare no competing interests.

Received: 11 December 2024 / Accepted: 25 February 2025
Published online: 12 March 2025

References

1. Agustí A, Melén E, DeMeo D, Breyer-Kohansal R, Faner R. Pathogenesis of chronic obstructive pulmonary disease: Understanding the contributions of gene-environment interactions across the lifespan. Lancet Respiratory Med. 2022;10:512–24.
2. Venkatesan P. GOLD COPD report: 2024 update. Lancet Respiratory Med. 2024;12:15–6.
3. Liang-Kung C, Jean W, Prasert A, Tung-Wai A, Ming-Yueh C, Katsuya I, Hak Chul J, Lin K, Miji K, Sunyoung K et al. Asian working group for sarcopenia: 2019 consensus update on sarcopenia diagnosis and treatment. J Am Med Dir Assoc, 21.
4. Leonardo MF, Bartolome RC, Alvar A, Gerard JC, Mark TD, Miguel D, Jamuna KK, Lies L, Maria MO, Sundeep SS et al. COPD and Multimorbidity: recognising and addressing a syndemic occurrence. Lancet Respir Med 2023, 11.
5. Yusheng C, Wei S, Jiaming L, Ying J, Chuqian L, Liyuan Z, Xia Z, Wenhui Z, Beibei L, Yongpan A et al. The landscape of aging. Sci China Life Sci 2022, 65.
6. Liao L, Deng M, Gao Q, Zhang Q, Bian Y, Wang Z, Li J, Xu W, Li C, Wang K, et al. Predictive and therapeutic value of lipoprotein-associated phospholipaseA2 in sarcopenia in chronic obstructive pulmonary disease. Int J Biol Macromol. 2024;275:133741.
7. Pauline H, Isabelle D, Pierre S, Pauline E, Léo B, Maéva Z, Fares G, Maurice H, Pascal P, Patrick B. Main pathogenic mechanisms and recent advances in COPD peripheral skeletal muscle wasting. Int J Mol Sci 2023, 24.
8. Sophie IJ, vB, Harry RG, Ramon CL, Annemie MWJS. Towards personalized management of sarcopenia in COPD. Int J Chron Obstruct Pulmon Dis 2021, 16.
9. Larsson L, Degens H, Li M, Salviati L, Lee Y, Thompson W, Kirkland J, Sandri M. Sarcopenia: Aging-Related loss of muscle mass and function. Physiol Rev. 2019;99:427–511.
10. Xie H, Wu L, Deng Z, Huo Y, Cheng Y. Emerging roles of YAP/TAZ in lung physiology and diseases. Life Sci. 2018;214:176–83.
11. Iwan S, Ardo S, Ronny L, Paul MY, Hanna G. Hippo pathway effectors YAP and TAZ and their association with skeletal muscle ageing. J Physiol Biochem 2021, 77.
12. Minyang F, Yuan H, Tianxia L, Kun-Liang G, Ting L, Min L. The Hippo signalling pathway and its implications in human health and diseases. Signal Transduct Target Ther, 7.
13. Watt KI, Turner BJ, Hagg A, Zhang X, Davey JR, Qian H, Beyer C, Winbanks CE, Harvey KF, Gregorevic P. The Hippo pathway effector YAP is a critical regulator of skeletal muscle fibre size. Nat Commun. 2015;6:6048.
14. Gnimassou O, Francaux M, Deldicque L. Hippo pathway and skeletal muscle mass regulation in mammals: A controversial relationship. Front Physiol. 2017;8:190.
15. Felipe SG, Adriana C-C, Alexia B-P, Daniela LR, Andrea R, Juan Carlos C, Enrique B. Denervation drives YAP/TAZ activation in muscular fibro/adipogenic progenitors. Int J Mol Sci 2023, 24.
16. Lidan Z, Yu-Taro N, Hiroyuki N, Takayuki K, Kazutake T, Madoka I-U, Akiyoshi U, Yoshiaki O, Takefumi D, Shuichi W et al. The CalcR-PKA-Yap1 Axis is critical for maintaining quiescence in muscle stem cells. Cell Rep 2019, 29.
17. Deng M, Zhang Q, Yan L, Bian Y, Li R, Gao J, Wang Y, Miao J, Li J, Zhou X, Hou G. Glycyl-l-histidyl-l-lysine-Cu(2+) rescues cigarette smoking-induced skeletal muscle dysfunction via a Sirtuin 1-dependent pathway. J Cachexia Sarcopenia Muscle. 2023;14:1365–80.
18. Zhang L, Li C, Xiong J, Chang C, Sun Y. Dysregulated myokines and signaling pathways in skeletal muscle dysfunction in a cigarette smoke-induced model of chronic obstructive pulmonary disease. Front Physiol. 2022;13:929926.
19. Li C, Deng Z, Zheng G, Xie T, Wei X, Huo Z, Bai J. Histone deacetylase 2 suppresses skeletal muscle atrophy and senescence via NF-κB signaling pathway in cigarette Smoke-Induced mice with emphysema. Int J Chron Obstruct Pulmon Dis. 2021;16:1661–75.
20. Alcalde-Estévez E, Sosa P, Asenjo-Bueno A, Plaza P, Valenzuela PL, Naves-Díaz M, Olmos G, López-Ongil S, Ruiz-Torres MP. Dietary phosphate restriction prevents the appearance of sarcopenia signs in old mice. J Cachexia Sarcopenia Muscle. 2023;14:1060–74.
21. Chen L, Luo L, Kang N, He X, Li T, Chen Y. The protective effect of HBO1 on cigarette smoke Extract-Induced apoptosis in airway epithelial cells. Int J Chron Obstruct Pulmon Dis. 2020;15:15–24.
22. Ko HK, Hsiao YH, Jeng MJ, Yang DM, Chen PK, Su KC, Chou KT, Perng DW. The role of transforming growth factor-β2 in cigarette smoke-induced lung inflammation and injury. Life Sci. 2023;320:121539.
23. Zhang L, Li D, Chang C, Sun Y. Myostatin/HIF2α-Mediated ferroptosis is involved in skeletal muscle dysfunction in chronic obstructive pulmonary disease. Int J Chronic Obstr Pulm Dis. 2022;17:2383–99.
24. Wang C, Yue F, Kuang S. Muscle histology characterization using H&E staining and muscle Fiber type classification using Immunofluorescence staining. Bio Protoc 2017, 7.
25. Sepúlveda-Loyola W, Osadnik C, Phu S, Morita A, Duque G, Probst V. Diagnosis, prevalence, and clinical impact of sarcopenia in COPD: a systematic review and meta-analysis. J cachexia Sarcopenia Muscle. 2020;11:1164–76.
26. Benz E, Trajanoska K, Lahousse L, Schoufour JD, Terzikhan N, De Roos E, de Jonge GB, Williams R, Franco OH, Brusselle G, Rivadeneira F. Sarcopenia in COPD: a systematic review and meta-analysis. Eur Respir Rev 2019, 28.
27. Li Y, Eugenie N, Marian V, Qinghua W, Kamil K. Mycotoxins and cellular senescence: the impact of oxidative stress, hypoxia, and immunosuppression. Arch Toxicol 2022, 97.
28. Nor Shaheera MK, Sabreena S, Shaharum S, Parisa F. Aging of the cells: insight into cellular senescence and detection methods. Eur J Cell Biol 2020, 99.
29. Sladitschek-Martens H, Guarnieri A, Brumana G, Zanconato F, Battilana G, Xiccato R, Panciera T, Forcato M, Bicciato S, Guzzardo V, et al. YAP/TAZ activity in stromal cells prevents ageing by controlling cGAS-STING. Nature. 2022;607:790–8.
30. Jiang Y, Fu L, Liu B, Li F. YAP induces FAK phosphorylation to inhibit gastric cancer cell proliferation via upregulation of HMGB1. Int J Biol Macromol. 2024;262:130037.
31. Murgia M, Toniolo L, Nagaraj N, Ciciliot S, Vindigni V, Schiaffino S, Reggiani C, Mann M. Single muscle Fiber proteomics reveals Fiber-Type-Specific features of human muscle aging. Cell Rep. 2017;19:2396–409.
32. Victoria M, Andrés C, Valentina S, Oleg D, Yiwei L, Sascha J, Eva A, Juan A, Jessica S, Laura O et al. Senescence atlas reveals an aged-like inflamed niche that blunts muscle regeneration. Nature 2022, 613.
33. Alexiane D, Jason DK, Shankar V, Andrea A. The cGAS-STING pathway as a therapeutic target in inflammatory diseases. Nat Rev Immunol 2021, 21.
34. Chenyu S, Zhuoyi H, Dingjun X, Huihui B, Juan L, Xuanxuan Z, Qiang Z, Li S, Heng Y, Tong L, Yinghua L. STING signaling in inflammaging: a new target against musculoskeletal diseases. Front Immunol 2023, 14.
35. Haarer E, Theodore C, Guo S, Frier R, Campellone K. Genomic instability caused by Arp2/3 complex inactivation results in micronucleus biogenesis and cellular senescence. PLoS Genet. 2023;19:e1010045.
36. Papalazarou V, Machesky L. The cell pushes back: the Arp2/3 complex is a key orchestrator of cellular responses to environmental forces. Curr Opin Cell Biol. 2021;68:37–44.
37. Ting X, Xinyue B, Xingyi W, Lezheng W, Fei L, Hui S, Yue S. Exercise rehabilitation and chronic respiratory diseases: effects, mechanisms, and therapeutic benefits. Int J Chron Obstruct Pulmon Dis 2023, 18.

38. Alfonso JC-J, Gülistan B, Jürgen B, Yves B, Olivier B, Tommy C, Cyrus C, Francesco L, Yves R, Avan Aihie S et al. Sarcopenia: revised European consensus on definition and diagnosis. Age Ageing 2019, 48.

Publisher's note